Biophysical Journal, Volume 99

Supporting Material

Experimental evolution of adenylate kinase reveals contrasting strategies towards protein thermostability

Corwin Miller, Milya Davlieva, Corey J. Wilson, Kristopher I. White, Rafael Counago, Gang Wu, Jeffrey C. Myers, Pernilla Wittung-Stafshede, and Yousif Shamoo

Supplementary Information

"Experimental evolution of adenylate kinase reveals contrasting strategies towards protein thermostability"

Corwin Miller, Milya Davlieva, Corey Wilson, Kristopher I. White, Rafael Couñago, Gang Wu, Jeffrey C. Myers, Pernilla Wittung-Stafshede and Yousif Shamoo

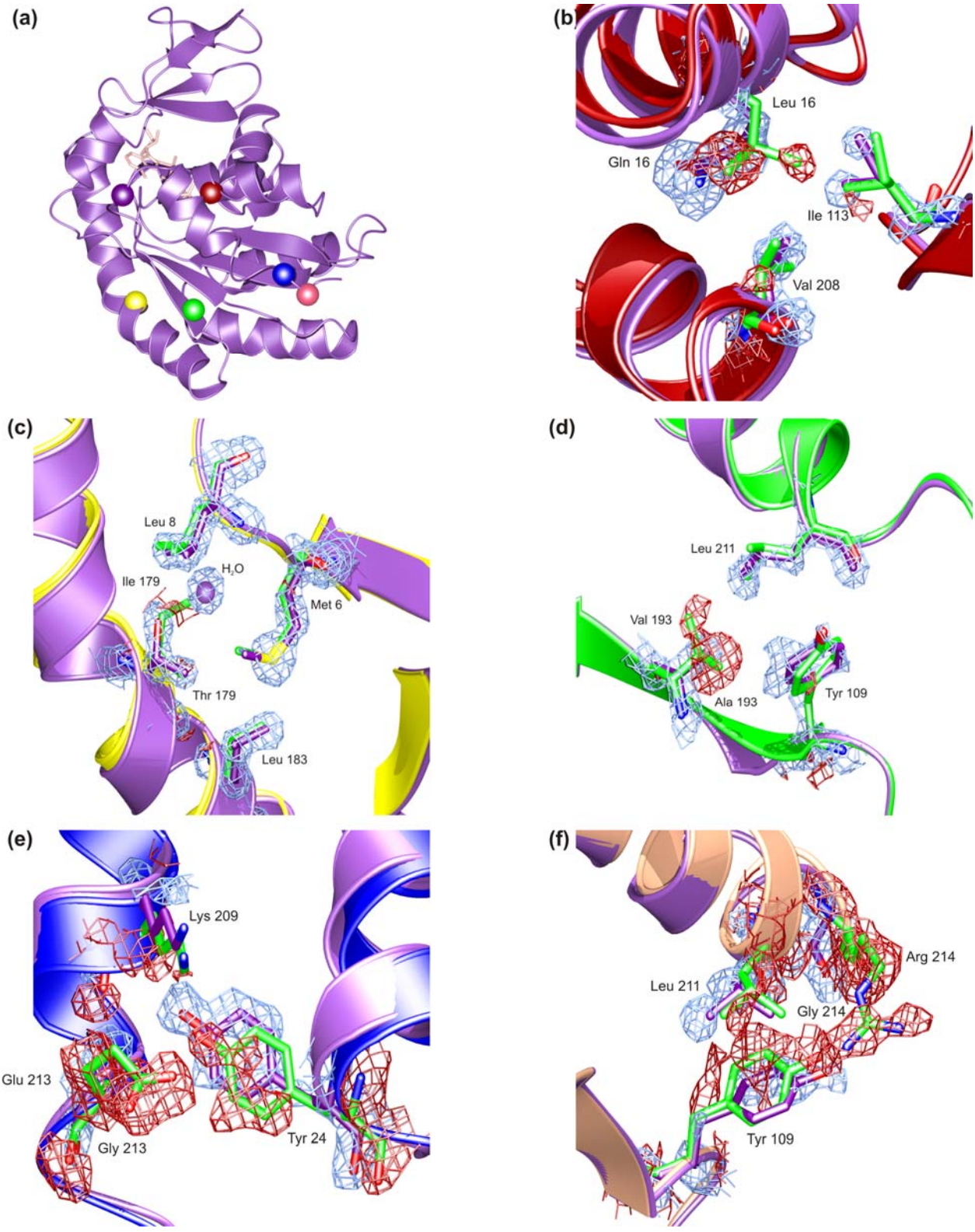

Supplementary Figure 1. Crystallographic analysis of adaptive AK_{BSUB} mutations at 1.8 Å resolution. (a) Secondary structure of AK_{BSUB} with the positions of mutations indicated as colored spheres: AK_{BSUB}Q199R/Q16L (red); AK_{BSUB}Q199R/T179I (yellow); AK_{BSUB}Q199R/A193V (green); AK_{BSUB}Q199R/G213E (blue) and AK_{BSUB}Q199R/G214R (orange). Secondary structure elements are labeled using the convention described by Bae and Phillips (2004)(1). (b-f) 2Fo-Fc difference density (2Fo-Fc AK_{BSUB} double mutant – 2Fo-Fc AK_{BSUB} Q199R) electron density maps covering the residues immediately surrounding the sites of each double mutant are shown in each panel. Positive density (blue). Negative density (red). The amino acids found originally in AK_{BSUB}Q199R are shown as purple sticks. (b) AK_{BSUB}Q199R/Q16L has excellent packing in a non-polar pocket made up of Leu-5, Ile-20,Ile-111, Ile-113, Val-204, Tyr-205 and Ala-206 (1.4 σ); (c) AK_{BSUB}Q199R/T179I displaces a water and packs into a non-polar pocket comprised of Met-6, Gly-7 and Leu-8 (1.4 σ); (d) AK_{BSUB}Q199R/A193V is at a largely solvent exposed position. Leu-211 and Tyr-109 are displaced slightly to form a pocket (1.9 σ); (e) AK_{BSUB}Q199R/G213E is in a highly solvent exposed position and may form a new electrostatic network made up of between Lys-209↔Glu-213↔Lys-216 along the solvent exposed face of the C-terminal helix-9 as well as Asp-23 from helix-1 (1.7 σ); and (f) AK_{BSUB}Q199R/G214R forms a new hydrogen bond to Tyr-109 potentially tethering the C-terminal helix to the core of the protein (1.3 σ).

Supplementary Table 1. Data collection and refinement statistics for AK_{BSUB} mutants					
Data collection	**Q199R/Q16L**	**Q199R/T179I**	**Q199R/A193V**	**Q199R/G213E**	**Q199R/G214R**
Wavelength (Å)	1.5418	1.5418	1.5418	1.5418	1.5418
Resolution (Å)	20.0-1.8	30.4-1.8	20.0-1.8	29.7-1.8	27.0-1.8
Space group	$P2_1$	$P2_1$	$P2_1$	$P2_1$	$P2_12_12_1$
Molecules per a.u.	2	2	2	2	1
Unit Cell (Å)	a =34.6	a=34.8	a =34.7	a =34.7	a=44.0
	b = 74.3	b=75.8	b = 75.1	b = 75.5	b=45.5
	c = 77.4	c=77.5	c = 77.5	c = 77.6	c=100.2
	β=100.2^o	β=98.2^o	β=98.6^o	β=98.9^o	$\alpha=\beta=\gamma$=90.0^o
Unique reflections	34,813	34,509	49,183	34,668	17,928
Completeness (%)[a]	96.1 (90.1)	93.4 (84.7)	94.8 (93.1)	94.7 (93.9)	95.8(92.2)
R_{merge} (%)[b]	5.7 (44.7)	2.1 (7.4)	5.2 (15.0)	5.7 (28.3)	3.2(10.4)
Refinement					
R_{work}/R_{free}[c]	24.5/26.4	19.7/24.5	22.8/26.89	22.7/27.3	19.8/23.9
r.m.s.d.					
bonds (Å)/angles (°)	0.010/1.40	0.005/1.22	0.008/1.40	0.005/1.20	0.008/1.40
Average B-factors (Å^2)					
main chain (A/B)	23.7/25.6	15.3/13.4	17.4/18.7	20.0/21.9	19.7
overall (A/B)	27.5/26.9	16.8/15.0	18.7/20.0	21.2/23.3	21.8
Ramachandran[d]					
favored (%)	93.1	95.0	95.3	93.7	96.2
disallowed (%)	0.0	0.0	0.0	0.0	0.0
PDB Accession Number	2osb	2oo7	2ori	2qaj	2p3s

[a] Parenthesis are values for highest resolution shell.
[b] $R_{merge} = \Sigma| I - \langle I \rangle | / \Sigma I$, where I is measured intensity for reflections with indices hkl.
[c] $R_{work} = \Sigma |F_o - F_c| / \Sigma |F_o|$ for all data with $F_o > 2 \sigma (F_o)$ excluding data to calculate R_{free} and $R_{free} = \Sigma |F_o - F_c| / \Sigma |F_o|$, for all data with $F_o > 2 \sigma (F_o)$ excluded from refinement.
[d] Calculated by using PROCHECK (2)

Supplementary Table 2. Comparison of AK_{BSUB} Mutant Structures						
	Q199R (A / B)	Q199R/ Q16L (A / B)	Q199R/ T179I (A / B)	Q199R/ A193V (A / B)	Q199R/ G213E (A / B)	Q199R/ G214R
Average main-chain B-factors ($Å^2$)	11.8/13.4	23.7/25.6	15.3/13.4	17.4/18.7	20.0/21.9	19.7
Average Overall B-factor ($Å^2$)	13.4/15.2	27.5/26.9	16.8/15.0	18.7/20.0	21.2/23.3	21.8
Number of ion pairs ($\leq$4Å cutoff)	26/26	27/27	27/23	23/23	22/25	23
Number of hydrogen bonds	123.4/126.5	120.8/122.6	122.3/125.8	126.1/126.2	123.3/123.4	126.9
Conditional Hydrophobic Accessible Surface Area ($Å^2$) (CHASA)[a]	4120/4135	4063/4277	4117/4103	4077/4112	4147/4036	4229
r.m.s.d. relative to AK_{BSUB} (Å)	0.71/0.60	0.72/0.63	0.68/0.64	0.71/0.64	0.73/0.70	0.49

[a] reference(3).

PDB entries used for comparative analyses are AK_{BSUB} (1P3J) (1), AK_{BSUB} Q199R - (2EU8) (4) and *Geobacillus stearothermophilus* AK (1ZIO) (5). Structures were aligned with O(6) or COOT using all Cα carbon positions. For determination of ion pairs using the program WHATIF two oppositely charged residues were included if their closest oppositely charged atoms were within a 4.0 Å cutoff(7). Carboxylic oxygen atoms of Asp, Glu and the C-terminal residue were considered as negatively-charged atoms; while amino nitrogen atoms of Arg, Lys, His and the N-terminal residue were treated as positively-charged atoms. Hydrogen bonds were estimated using the HB2 options in WHAT IF were used to define hydrogen bonds(7). In HB2, the total hydrogen bonding energy is optimized to find the optimal positions for all hydrogen atoms simultaneously, and hydrogen bonds are determined from the

donor/acceptor types, the H-acceptor distance, the donor-H-acceptor angle and the position of the hydrogen with respect to the acceptor. The conditional hydrophobic accessible surface area (CHASA) was determined (3). All figures with molecular structures were generated using CCP4MG or PyMOL(8-10).

Supplementary Table 3. Hydrogen isotope exchange rate of AK_{BSUB} mutants.

Protein	K_1 [min^{-1}]	K_2 [min^{-1}]
B. subtilis WT	0.129±0.004	0.005±0.001
AK_{BSUB} Q199R	0.127±0.02	0.004±0.0006
AK_{BSUB} Q199R/G213E	0.140±0.002	0.007±0.001
AK_{BSUB} Q199R/T179I	0.133±0.006	0.004±0.001
AK_{BSUB} Q199R/G214R	0.127±002	0.007±0.001
AK_{BSUB} Q199R/A193V	0.208±0.04	0.006±0.0007
AK_{BSUB} Q199R/Q16L	0.137±0.0002	0.005±0.0005
B. subtilis WT + AP5A	0.100±0.002	0.004±0.0006

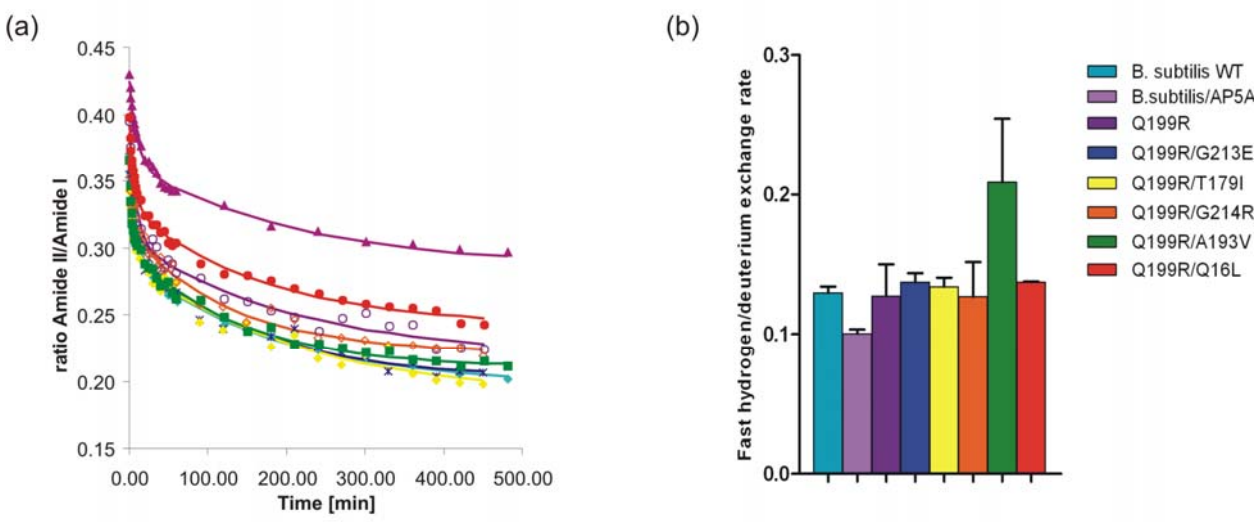

Supplementary Figure 2. Fourier-transformed infrared (FT-IR) spectroscopy shows a faster rate of deuterium exchange for AK_{BSUB}Q199R/A193V than the other adaptive mutations to AK_{BSUB}. (a) Change in the ratio of Amide II to Amide I peaks for AK_{BSUB} mutants over time during hydrogen/deuterium exchange monitored by FT-IR. The line represents the best fit of double-exponential decay curve during the time course of the experiment (7.5-8 hours at 22 ºC). (b) The difference in the fast hydrogen/deuterium exchange rate of the AK mutants at 22 ºC with the error bar showing the standard deviation.

FT-IR Studies - Hydrogen isotope exchange to probe protein flexibility. Fourier-transformed infrared (FT-IR) spectroscopy was used to provide a measure of the global hydrogen exchange rate of the AK_{BSUB} mutants at 22 ^{o}C. The absorption associated with Amide I arose from the in-plane C=O stretching vibration weakly coupled with C-N stretching and in-plane N-H bending. The Amide II is primary N-H bending strongly coupled with C-N stretching(11, 12). The Amide I band is slightly influenced during H/D exchange, which makes it a good internal standard for protein concentration(13). Thus, for each spectrum, the ratio of the amide II peak (centered at approximately 1550 cm^{-1}) to the amide I peak (centered at approximately 1655 cm^{-1}) was determined (Supplementary Figure 2). The change in this ratio with time after addition of D_2O is a convenient measure for the estimation of the rate of exchange of internal amide hydrogens with solvent deuterons. The resultant decay plots were fitted with a two-exponential model to produce

a smoothed curve (Supplementary Figure 2 and Table 3). The exponents of these curves were taken as rate constants which represent the major population of amide hydrogens exchanging during the time course of the experiment (14, 15). FT-IR data reveal that the rate constant for fast and slow exchanging amide protons does not substantially change for all AK mutants with the exception of AK_{BSUB} Q199R/A193V. AK_{BSUB} Q199R/A193V has a 2-fold change in the fast exchange rate consistent with the protein folding kinetics described previously. As a control for the sensitivity of the FT-IR experiment in sensing a potential change in AK dynamics we measured the exchange rate of wild type AK_{BSUB} bound to the inhibitor Ap5A that would stabilize the closed conformation of the LID domain of AK and presumably reduce the overall exchange rate (16, 17). In the presence of Ap5A, the exchange did decrease modestly and suggests that the almost two-fold change in exchange rate for AK_{BSUB} Q199R/A193V is consistent with a more dynamic structure.

The infrared spectra were measured with a Nicolet Nexus 470 (Thermo Electron-Nicolet, Waltham, MA) Fourier transform infrared spectrometer. The sample chamber of the spectrophotometer was purged constantly with nitrogen gas for at least 24 hours prior to the experiments and during data collection. Protein samples for H/D exchange experiments were dialyzed in 10 mM sodium phosphate buffer solution, pH 7.0 and lyophilized above liquid nitrogen to dryness. Lyophilized samples were reconstituted by dissolving in D_2O water to produce a 1 mM protein solution in 10 mM sodium phosphate buffer and were injected immediately into a CaF_2 cell with a 40 μm Teflon spacer. Spectra were recorded at 1, 2, 3, 4, 5, 6, 7, 8, 9, 10, 20, 30, 40, 50, 60 min after initiating the H/D exchange and every 30 min thereafter up to 450 min. A total 34 scans with a resolution of 2 cm^{-1} were collected and averaged for each time interval. The water vapor background spectrum was subtracted from each

sample spectrum. Spectra collection, averaging and subtraction were performed using the OMNIC software (version 7.1a, Thermo Electron Corporation)

Additional Materials and Methods

Protein Expression and Purification – Site-directed mutagenesis of wild type *B. subtilis* adenylate kinase (Sequence ID Z99104.2) in the pET-11a vector (Novagen, NJ, USA) was performed using the Stratagene QuikChange™ Site-Directed Mutagenesis Kit (Stratagene, La Jolla, CA, USA) as per the manufacturer's protocol. The plasmid containing the wild type *B. subtilis adk* gene was the generous gift of Dr. G. N. Phillips (U. Wisconsin at Madison). All clones were confirmed by DNA sequencing. Proteins were overexpressed and purified from *E. coli* as previously described (4).

REFERENCES

1. Bae, E., and G. N. Phillips, Jr. 2004. Structures and analysis of highly homologous psychrophilic, mesophilic, and thermophilic adenylate kinases. J Biol Chem 279:28202-28208.
2. Laskowski, R. A., M. W. MacArthur, D. S. Moss, and J. M. Thornton. 1993. PROCHECK: a program to check the stereochemical quality of protein structures. J. Appl. Crystallogr. 26:283-291.
3. Fleming, P. J., N. C. Fitzkee, M. Mezei, R. Srinivasan, and G. D. Rose. 2005. A novel method reveals that solvent water favors polyproline II over beta-strand conformation in peptides and unfolded proteins: conditional hydrophobic accessible surface area (CHASA). Protein Sci 14:111-118.
4. Counago, R., S. Chen, and Y. Shamoo. 2006. In vivo molecular evolution reveals biophysical origins of organismal fitness. Mol Cell 22:441-449.
5. Berry, M. B., and G. N. Phillips. 1998. Crystal Structures of Bacillus stearothermophilus Adenylate Kinase With Bound Ap_5A, Mg^{2+} Ap_5A, and Mn^{2+} Reveal an Intermediate Lid Position and Six Coordinate Octahedral Geometry for Bound Mg^{2+} and Mn^{2+}. Prot. Struc. Func. Genet. 32:276-288.
6. Jones, T. A., J.-. Zou, Y., S. W. Cowan, and M. O. Kjeldgaard. 1991. O. Acta Crystallogr A47:110-119.
7. Vriend, G. 1990. WHAT IF: a molecular modeling and drug design program. J Mol Graph 8:52-56, 29.
8. Potterton, E., S. McNicholas, E. Krissinel, K. Cowtan, and M. Noble. 2002. The CCP4 molecular-graphics project. Acta Crystallogr D Biol Crystallogr 58:1955-1957.

9. Potterton, L., S. McNicholas, E. Krissinel, J. Gruber, K. Cowtan, P. Emsley, G. N. Murshudov, S. Cohen, A. Perrakis, and M. Noble. 2004. Developments in the CCP4 molecular-graphics project. Acta Crystallogr D Biol Crystallogr 60:2288-2294.
10. DeLano, W. L. 2002. The PyMol Molecular Graphics System. DeLano Scientific, San Carlos.
11. Susi, H. 1972. Infrared spectroscopy--conformation. Methods Enzymol 26 PtC:455-472.
12. Haris, I. P., and F. Severcan. 1999. FTIR spectroscopic characterisation of protein structure in aqueous and non-aqueous media. . J. Mol. Catalysis B: Enzymatic 7:207-221.
13. Ottesen, M. 1971. Methods for measurement of hydrogen isotope exchange in globular proteins. Methods Biochem Anal 20:135-168.
14. Fields, A. P., Y. Kim, F. J. Carpenter, and N. G. Somero. 2002. Temperature adaptation in *Gillichthys* (Teleost: Gobiidae) A_4-lactate dehydrogenases: identical primary structures produce subtly different conformations. . J. Exper. Biol. 205:1293-1303.
15. Zavodszky, P., J. Kardos, and G. A. Petsko. 1998. Adjustment of conformational flexibility is a key event in the thermal adaptation of proteins. Proc. Natl. Acad. U.S.A. 95:7406-7411.
16. Shapiro, Y. E., M. A. Sinev, E. V. Sineva, V. Tugarinov, and E. Meirovitch. 2000. Backbone dynamics of escherichia coli adenylate kinase at the extreme stages of the catalytic cycle studied by (15)N NMR relaxation. Biochemistry 39:6634-6644.
17. Shapiro, Y. E., E. Kahana, V. Tugarinov, Z. Liang, J. H. Freed, and E. Meirovitch. 2002. Domain flexibility in ligand-free and inhibitor-bound Escherichia coli adenylate kinase based on a mode-coupling analysis of 15N spin relaxation. Biochemistry 41:6271-6281.